ACS Catalysis

pubs.acs.org/acscatalysis
Research Article

Partially Bonded Aluminum Site on the External Surface of Post-treated Au/ZSM-5 Enhances Methane Oxidation to Oxygenates

Jingxian Cao, Guodong Qi, Bingqing Yao, Qian He, Richard J. Lewis, Xu Li, Feng Deng, Jun Xu,* and Graham J. Hutchings*

Cite This: ACS Catal. 2024, 14, 1797−1807
Read Online

ACCESS | Metrics & More | Article Recommendations | Supporting Information

ABSTRACT: Au nanoparticles supported on the exterior surface of the ZSM-5 zeolite (Au/ZSM-5) have shown the ability to partially oxidize methane to methanol and acetic acid. However, further improvements to the catalyst activity are required. This study investigates the effect of modifying the acidic properties of the ZSM-5 support through a desilication−recrystallization (DR) process on the activity of Au/ZSM-5 catalysts toward methane oxidation. A DR treatment of 24 h leads to a 50% higher oxygenate yield compared to the analogous catalyst prepared using the untreated support. Characterization using solid-state ^{27}Al NMR and FTIR adsorption of pyridine and 2,4,6-trimethylpyridine reveals that DR induces framework dealumination and redistribution of Brønsted acid sites to the zeolite external surface. Two-dimensional ^{27}Al MQMAS NMR further identifies partially coordinated framework Al sites on the zeolite surface, correlating with a higher oxygenate yield. These external acid sites help stabilize the Au nanoparticles, enhancing catalyst stability for methane partial oxidation.

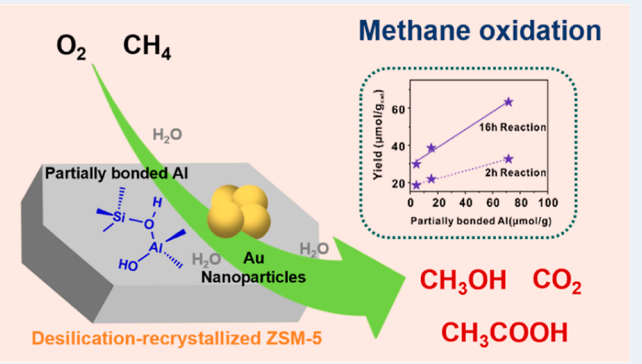

KEYWORDS: *methane oxidation, oxygenates, Au nanoparticles, zeolite, acid sites*

INTRODUCTION

The conversion of methane to value-added fuels/chemicals is of great academic and industrial interest.[1−4] Since methane has a stable tetrahedron structure and high C−H bond energy (439 kJ/mol),[5−7] the activation and conversion of methane are thermodynamically challenging. Currently, on an industrial scale, methane is converted into chemicals using an indirect route, involving the reforming of methane to syngas (a mixture of CO and H_2), which is subsequently utilized in the formation of oxygenated products via Fischer−Tropsch synthesis (FTS).[8] This indirect route necessitates high temperatures (up to 1000 °C) and pressures (up to 30 bar) with considerable associated energy demands. Hence, developing alternative processes, where methane is activated efficiently under mild conditions has become an area of intense research attention in recent years.[9−14]

The direct conversion of methane to oxygenated products in the liquid-phase under low-temperature conditions requires strongly acidic media such as oleum[5,15] in a homogeneous system. Previous studies have shown that electrophilic metals such as Hg and Pt-complexes are active catalysts for methane oxidation.[5,15] However, the homogeneous system has several drawbacks, such as the use of highly corrosive reagents (e.g., sulfuric acid and trifluoroacetic acid), the difficulty of separating the methanol product from the solvent, and substantial environmental impacts. Therefore, researchers have explored heterogeneous catalytic systems as an alternative approach.[16−18] H_2O_2 is a potent oxidant for methane conversion over various heterogeneous catalysts,[19−24] but its low utilization efficiency (due to its rapid decomposition) and its high cost limits application in methane selective oxidation processes. However, recent investigations have reduced the cost barrier to the use of H_2O_2 through its synthesis in situ from H_2 and O_2 over ZSM-5-encapsulated AuPd alloys, although considerable improvements in reactivity are still required.[25] Molecular oxygen may be considered an ideal oxidant for methane conversion, but it has low efficacy in mild conditions, requiring the use of coreductants, such as H_2 and CO to enhance methane oxidation rates.[26,27] In particular, Flytzani-Stephanopoulos and co-workers have demonstrated the efficacy of Rh/ZSM-5 catalysts for methane oxidation using O_2 in the presence of CO, with high selectivity toward acetic acid observed.[18]

Received: October 20, 2023
Revised: December 6, 2023
Accepted: December 6, 2023

https://doi.org/10.1021/acscatal.3c05030
ACS Catal. 2024, 14, 1797−1807

Cu-zeolites have also been reported to exhibit significant activity in the partial oxidation of methane to methanol using O_2 as an oxidant.[6,28−31] The methanol productivity of Cu-zeolites is highly dependent on the catalyst preparation strategies and catalytic routes, which are influenced by the properties of the zeolitic support.[32,33] Cu-modified ZSM-5 and MOR zeolites catalysts can utilize a two-stage catalytic cycle to form methanol,[32,34,35] in which a surface methoxyl group is first formed on the oxidized Cu species and then extracted as methanol at a lower temperature with water. Various Cu sites, such as mono(μ-oxo) dicopper, trinuclear, and larger copper oxygen clusters were reported to be formed depending on the structure of the zeolite, with the method of introduction of the Cu species, and post-thermal treatment, significantly affecting catalytic performance. In particular, it was found that methanol productivity increased linearly with the Cu/Al ratio and varied with the Si/Al ratio.[36] Recently, Qi and co-workers reported that Au nanoparticle-supported ZSM-5 catalyst can enable direct catalytic conversion of methane to methanol and acetic acid in water at temperatures between 120 and 240 °C using O_2 and in the absence of any coreductant.[37] It was demonstrated that oxygen was activated on Au nanoparticles and the acidity of zeolite facilitated methane activation to reactive CH_3 species for further transformations.[37] However, as with many approaches to methane valorization, considerable improvements in oxygenate productivity are still required to rival the current industrial process.

In this study, we investigate the oxidation of methane using Au/ZSM-5 catalysts with modified zeolite acidity. This is achieved through a desilication−recrystallization (DR) treatment of the ZSM-5 support prior to the immobilization of Au species via a deposition−precipitation method (Scheme S1). We explore the impact of the DR treatment on the activity and stability of the Au/ZSM-5 catalysts. The modified catalyst demonstrates a 50% increase in oxygenate yield (mainly through the increased formation of methanol and acetic acid), compared to the unmodified catalyst. We show that the location of Brønsted acid sites (BASs) influences the activity of Au/ZSM-5 in methane oxidation, with partially bonded Al sites on the external surface of ZSM-5 promoting both catalyst activity and stability.

EXPERIMENTAL METHODS

Note on Safe Operation of Experiments. Any reaction involving catalytic oxidation must work under conditions outside of the explosive mixture composition of the reagents. The preparation of Au-supported ZSM-5 catalysts was handled in small quantities (less than 1 g) to avoid the explosion of fulminating gold, which might be yielded by the reaction of ammonia and hydrogen tetrachloroaurate(III).[38] In the case of the methane oxidation reaction, Cooper and Wiezevich have shown that as long as the experiments are conducted at ≤14% O_2, even at elevated temperature and pressure, the experiment is outside of the explosive regime.[39] This is the case for all experiments reported in this work.

DR Treatment of ZSM-5 Zeolite. The ZSM-5 (Si/Al = 13.5, Nankai University Catalyst Co., Ltd.) powder was calcined at 550 °C for 6 h in static air with a ramp rate of 3 °C/min from room temperature to 550 °C. Then, ZSM-5 (4 g, calcined) was mixed with tetra-propylammonium hydroxide (TPAOH) solution (3.25 g, 25%, Sinopharm Chemical Reagent Co.) and deionized (DI) water (37 mL) at 500 rpm for 20 min to form a slurry. The slurry was transferred into a PTFE-lined autoclave and heated at 160 °C for different times (6−72 h) under autogenous pressure without stirring. After the desired time, the vessel was allowed to cool to ambient temperature, and the resulting solid was filtered, washed with around 150 mL of DI water, dried (120 °C, 16 h), and calcined (550 °C, 6 h). The resulting product was denoted as ZSM-5(DR-x) (x represents the post-treatment time in h). The ZSM(DR-24) were washed with ammonium hexafluorosilicate (AHFS) by dispersing the samples in AHFS solution at a concentration of 1 g/10 mL with an AHFS: Al ratio of 4 [denoted as ZSM(DR-24-AHFS)]. The mixture was heated to 90 °C under vigorous agitation. After 5 h of stirring, the final mixture was filtered and washed three times with 1 L of deionized water; subsequently, the samples were dried in air at 100 °C overnight and then calcined at 550 °C for 6 h in static air with a ramp rate of 2 °C/min from room temperature to 550 °C.

Preparation of Au-Supported ZSM-5 Zeolites. 0.25−2 wt % Au-loaded Au/ZSM-5(DR-x, x: 6−72 h) catalysts were prepared by a deposition−precipitation method following a previous report.[37] Typically, the zeolite (1.0 g) was dispersed in DI water (67 mL) and mixed with a known amount of $HAuCl_4$ aqueous solution (6.0 mmol/L, $HAuCl_4{\cdot}3H_2O$, ≥49.0% Au basis, Merck) under vigorous stirring. A suitable volume of 2.5 wt % aqueous ammonia solution was gradually added to the above solution until the pH value of 6 was reached, which took more than 30 min at room temperature. The resulting solution was aged in a preheated water bath at 60 °C for 2 h under stirring at 600 rpm. Then, the sample was filtered and thoroughly washed with around 300 mL of deionized water. After drying in an oven at 60 °C (16 h), the sample was further calcined in a tubular furnace in static air. The temperature was programmed from room temperature to 240 °C at 3 °C/min and held at 240 °C for 90 min and then cooled to room temperature. The same procedure was used to prepare Au/ZSM-5 using the untreated zeolite for comparison (Table S1).

Characterization. *X-ray Diffraction.* Powder X-ray diffraction (XRD) was performed on a PANAlytical X'Pert Powder X-ray diffraction diffractometer with Cu Kα (λ = 1.5406 Å), recording at 40 kV and 40 mA. The scan rate is 0.2 deg/s.

Fourier Transform Infrared. The acidity of the prepared catalysts was measured by Fourier transform infrared (FT-IR) transmittance of pyridine and 2,4,6-trimethylpyridine adsorption experiments. The measurements were carried out on a Bruker Tensor 27 spectrometer. The samples were pretreated under vacuum (<2 Pa) at 473 K for 3 h. After cooling down to 303 K, a background spectrum was recorded. Then the samples were exposed to saturated adsorption pyridine or 2,4,6-trimethylpyridine for 10 min to reach equilibrium. Physiosorbed pyridine or 2,4,6-trimethylpyridine was removed by evacuation at 473 K for 2 h. The band area at 1515−1565 cm^{-1} and 1435−1470 cm^{-1} was used to quantify the concentration of BASs and Lewis acid sites (LASs), respectively.

Inductively Coupled Plasma Optical Emission Spectroscopy. The Au content of the Au/ZSM-5(DR-x) samples was analyzed using an Agilent ICP-OES 730 inductively coupled plasma optical emission spectrometer.

Transmission Electron Microscopy. High-angle annular dark-field imaging was performed by using an aberration-

https://doi.org/10.1021/acscatal.3c05030
ACS Catal. 2024, 14, 1797−1807

corrected JEOL ARM200CF microscope equipped with a cold field-emission gun operating at 200 kV.

Solid-State NMR. ^{29}Si solid-state NMR experiments were carried out at 11.7 T on a Bruker Avance III 500 spectrometer equipped with a 7 mm probe with resonance frequencies of 99.45 MHz. The magic angle spinning rate was set to 5 kHz. The hpdec ^{29}Si MAS NMR experiments were performed using a ^{29}Si 45° pulse length of 3.65 μs and a recycle delay of 30 s. The ^{29}Si chemical shifts were referenced to kaolinite (−91.5 ppm).

^{27}Al solid-state NMR experiments and two-dimensional (2D) ^{27}Al multiple-quantum (MQ) z-filtering NMR experiments were carried out on an 18.8 T Bruker Avance III spectrometer using a 3.2 mm double-resonance probe with an MAS spinning rate of 20 kHz. The resonance frequency of ^{27}Al was 208.5 MHz. The ^{27}Al MAS NMR spectra were acquired using a small-flip angle technique with a pulse length of 0.5 μs ($<\pi/6$) and a recycle delay of 0.5 s. For the 2D ^{27}Al 3Q MAS z-filtering NMR experiment, the z-filter pulse sequence was used with high-power ($\upsilon_{RF} \approx 191$ kHz) excitation (0Q → ± 3Q) and conversion pulses (±3Q → 0Q) of 5.6 and 1.5 μs, respectively. The "soft" $\pi/2$ pulse (0Q → −1Q) was set to 16 μs with $\upsilon_{RF} \approx 16$ kHz. All spectra had a recycle delay of 0.2 s. The ^{27}Al chemical shifts were referenced to 1 M Al $(NO_3)_3$ aqueous solution (0 ppm). ^{27}Al solid-state NMR and 2D ^{27}Al MQMAS NMR experiments were also carried out on an 11.7 T Bruker Avance III spectrometer using a 4 mm double-resonance probe with an MAS spinning rate of 12.5 kHz. The resonance frequency of ^{27}Al was 130.4 MHz. The ^{27}Al MAS NMR spectra were acquired using a small-flip angle technique with a pulse length of 0.2 μs ($<\pi/6$) and a recycle delay of 0.5 s. For the 2D ^{27}Al 3Q MAS z-filtering NMR experiment, the z-filter pulse sequence was used with high-power ($\upsilon_{RF} \approx 209$ kHz) excitation (0Q→ ± 3Q) and conversion pulses (±3Q → 0Q) of 5.6 and 2.0 μs, respectively. The "soft" $\pi/2$ pulse (0Q → −1Q) was set to 16 μs with $\upsilon_{RF} \approx 16$ kHz. All spectra had a recycle delay of 0.2 s. The ^{27}Al chemical shifts were referenced to 1 M Al $(NO_3)_3$ aqueous solution (0 ppm). The single-pulse ^{27}Al MAS spectra were fitted using a quadrupolar line shape with a Cz simple model in the DMFIT software.[40] The fittings accounted for the centers of gravity in the F1 and F2 dimensions as well as the isotropic chemical shifts and quadrupolar product parameters obtained from the ^{27}Al MQMAS NMR spectra.

Methane Oxidation. Methane oxidation with oxygen was carried out in a stainless-steel Parr autoclave (25 mL) without a liner. In general, the catalyst (0.1 g) and DI water (15 mL) were transferred into the reactor, which was then sealed and bubbled with pure nitrogen for more than 30 min to remove the dissolved gas in water. After being purged three times with methane, the reactor was pressurized with a gas mixture of methane and oxygen. The total pressure was set at 24.2 bar with varied methane and oxygen partial pressures (0.14−3.5 bar) at room temperature. The mixture was stirred at 1000 rpm for 5 min at room temperature, and the pressure remained constant at 24.2 bar. Subsequently, the reactor was heated to the desired reaction temperature (120−240 °C) within 40 min and maintained at the reaction temperature for 32 min to 32 h under a stirring rate of 1000 rpm. The reaction was stopped by cooling in ice water to a temperature below 10 °C in order to minimize the loss of volatile products. The reaction gas was released into a gas sampling bag.

The liquid products were sampled using a glass syringe with a Teflon filter head for NMR analysis. The gaseous product analysis was performed on a Shimadzu GC-2014C gas chromatography system equipped with a methanizer unit and FID detector using a TDX-01 packed column. The liquid products were quantified by ^{1}H NMR on a Bruker Avance-500 liquid NMR spectrometer using a water suppression pulse sequence (Watergate5). The measurement was calibrated by using CH_3CN as an internal standard.

RESULTS AND DISCUSSION

Structural Characterization of the Fresh Catalysts. The crystal structures and gold species of the prepared Au/ZSM-5 catalysts with different DR treatments were characterized by powder XRD and high-angle annular dark-field scanning transmission electron microscopy (HAADF-STEM). XRD patterns (Figure 1a) reveal the MFI framework remains

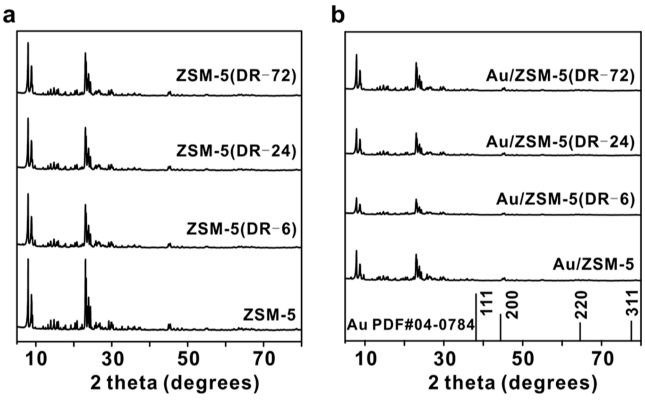

Figure 1. XRD patterns of (a) ZSM-5 and DR-treated ZSM-5 supports and (b) Au-supported ZSM-5 and DR-treated ZSM-5 catalysts.

stable after DR, as no significant changes were observed compared to the reference ZSM-5 sample. This was further confirmed by solid-state ^{29}Si MAS NMR analysis (Figure S1). Although bulk Au peaks are not detected in the XRD of any samples (Figure 1b), likely due to the formation of well-dispersed nanoscale particles, HAADF-STEM micrographs (Figure 2) show the presence of Au particles greater than 6 nm on all fresh catalysts, consistent with our recent report.[37] No isolated Au atoms or subnanometer clusters were observed. Average Au particle sizes are estimated from HAADF-STEM analysis to be 9.6 nm (±1.2 nm) for Au/ZSM-5(DR-6), 9.1 nm (±1.2 nm) for Au/ZSM-5(DR-24), 9.8 nm (±0.9 nm) for Au/ZSM-5(DR-72), and 10.1 nm (±1.0 nm) for the Au/ZSM-5 catalyst without DR. These similar particle sizes suggest DR does not impact the initial state of supported Au, which is primarily nanoparticulate in nature. Overall, complementary XRD and STEM characterization reveals that the crystallinity and framework of the DR-treated ZSM-5 support, as well as the nanoscale morphology of dispersed Au species, remained largely unchanged by DR treatments.

Methane Oxidation Reactions on Au/ZSM-5 with DR Treatment. The direct oxidation of CH_4 was performed on the Au/ZSM-5(DR-x) catalysts, with comparrions made to the catalyst without DR treatment (Figure 3 and Table S2). In Figure 3a, the yield and selectivity of methane oxidation are examined over various catalysts in water under optimized conditions: 2 h at 240 °C, with 3.5 bar O_2 and 20.7 bar CH_4

https://doi.org/10.1021/acscatal.3c05030
ACS Catal. 2024, 14, 1797−1807

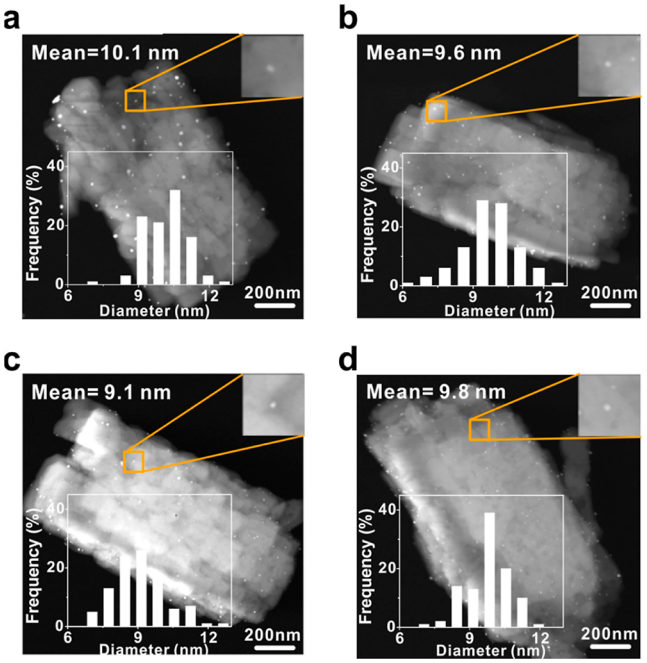

Figure 2. HAADF-STEM characterization of various fresh catalysts with 0.5 wt % Au loading and their corresponding particle size distributions. (a) Au/ZSM-5, (b) Au/ZSM-5(DR-6), (c) Au/ZSM-5(DR-24), and (d) Au/ZSM-5(DR-72).

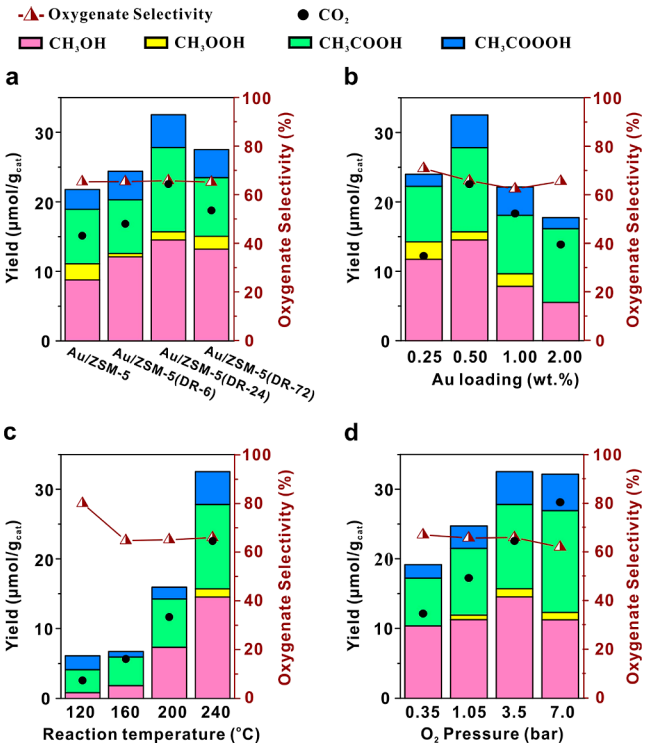

Figure 3. Methane oxidation on 0.5 wt % Au-loading zeolites prepared with different DR time (a) and Au/ZSM-5(DR-24) catalysts with different Au-loading (b). The effect of reaction temperature (c) and O_2 partial pressure (d) on methane oxidation of Au/ZSM-5(DR-24) sample with 0.5 wt % Au-loading. Reaction conditions: catalyst (0.1 g), CH_4 (20.7 bar), O_2 (3.5 bar) 120 min, H_2O (15 mL), 240 °C, for (c) the reaction temperature varied from 120 to 240 °C and for (d) O_2 partial pressure varied from 0.35 to 7.0 bar and the total reaction pressure was kept at 24.2 bar by CH_4.

charged at room temperature. These conditions have been established as the optimum for CH_4 oxidation on Au/ZSM-5 catalyst, as reported in our previous studies.[37,41] The identification of liquid oxygenate products, including methanol, methyl hydroperoxide, acetic acid, and peracetic acid, was performed through quantitative ^{1}H NMR analysis. Overall, the DR-treated samples exhibit improved oxygenate yield compared with the unmodified Au/ZSM-5 catalyst. However, the selectivity of oxygenates remains constant at approximately 65%, suggesting that the DR treatment of the zeolite support does not alter the reaction pathways.[37] The highest oxygenate yield of 32.5 μmol/g_{cat} is observed with the Au/ZSM-5(DR-24) catalyst, representing a 50% enhancement when compared with the Au/ZSM-5. These results indicate that the DR treatment of the zeolite support is beneficial for the Au-supported catalyst in methane oxidation. The optimal Au loading amount was determined for the Au/ZSM-5(DR-24) catalyst. Figure 3b illustrates methane oxidation catalyzed by Au/ZSM-5(DR-24) with varying Au loadings ranging from 0.25 to 2.0 wt %. The yield of oxygenates increased with increasing Au loading up to 0.5 wt % but declined as the Au loading further increased to 2.0 wt %. TEM analysis reveals significant agglomeration of Au particles at high Au loading (Figure S2). The selectivity of oxygenates is only slightly affected by the variation in the Au loading. Additionally, the effects of reaction temperature and O_2 partial pressure on methane oxidation were investigated using the Au/ZSM-5(DR-24) catalyst with 0.5 wt % Au loading. As depicted in Figure 3c, higher temperatures significantly enhance methane oxidation, while lower temperatures facilitate higher selectivity toward oxygenates, possibly due to the restriction of methane overoxidation to CO_2. The variation in the pressure of the O_2 demonstrates that higher pressure of the O_2 leads to increased liquid oxygenate yield, albeit with a slight decrease in selectivity (Figure 3d). This observation may be attributed to the overoxidation of liquid oxygenates under high-oxygen atmospheres.

To investigate the impact of DR treatment on the catalyst stability in methane oxidation, reactions were conducted using both Au/ZSM-5(DR-24) and Au/ZSM-5 catalysts over an extended reaction time. Figure 4a–c presents the results of time-on-line analysis, revealing the consecutive formation of products (including liquid- and gas-phase products) and a similar trend in liquid oxygenate selectivity over a 2000 min reaction period. During the initial stage of methane oxidation (before 400 min), both catalysts exhibit considerable activity toward oxygenate synthesis. However, the Au/ZSM-5(DR-24) sample demonstrates faster reaction rates than the Au/ZSM-5 sample, evident in both the liquid- and gas-phase products. The reaction tends to stabilize in the later stage (after 1000 min), although a minor decrease in methane oxidation products is observed over the Au/ZSM-5(DR-24) catalyst at extended reaction times (Figure 4a,b). Notably, for both catalysts, oxygenate selectivity in excess of 40% is observed over the full 2000 min reaction period (Figure 4c). ICP analysis confirms minimal leaching of Au on the catalyst during extended reaction periods, as demonstrated by the Au content of 0.41 wt % in the fresh catalyst and 0.38 wt % in the used catalyst (after 960 min of reaction) of Au/ZSM-5(DR-24). The XRD analysis reveals that the MFI framework is well-preserved (Figure S3). These data suggest that the Au/ZSM-5(DR-24) catalyst possesses strong stability during methane oxidation. To further assess the stability of the Au/ZSM-5(DR-

https://doi.org/10.1021/acscatal.3c05030
ACS Catal. 2024, 14, 1797−1807

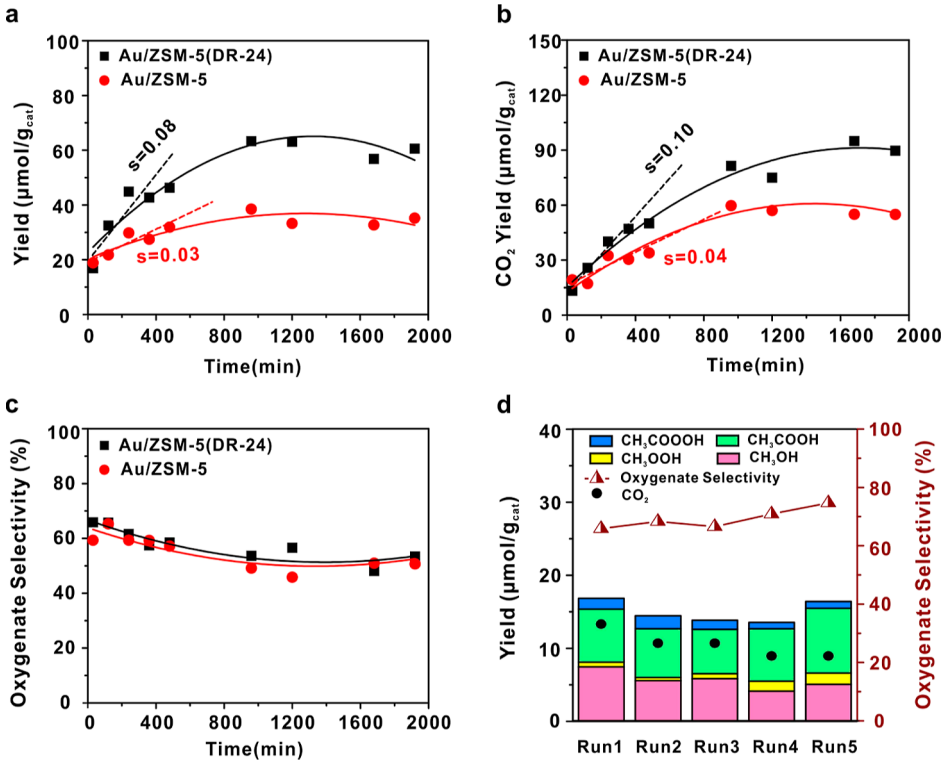

Figure 4. Liquid oxygenate yield (a), gas-phase CO_2 yield (b), and liquid oxygenate selectivity (c) using different reaction times and catalyst reuse experiments (d) of methane oxidation on Au/ZSM-5(DR-24) catalyst. Reaction conditions: catalyst (0.1 g), CH_4 (20.7 bar), O_2 (3.5 bar), and H_2O (15 mL) 240 °C. For reuse experiments, after each run the catalyst was dried (60 °C, 16 h) and calcined (240 °C, 1.5 h) prior to the next run and for each run the catalyst reaction time was 30 min.

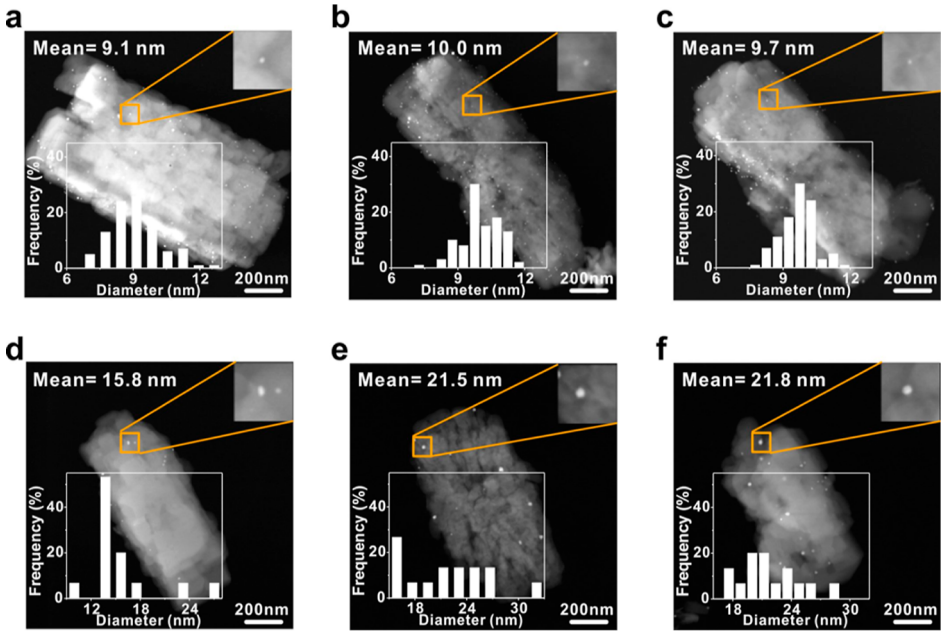

Figure 5. HAADF-STEM images of fresh catalysts and used samples after different reaction times: (a) fresh Au/ZSM-5(DR-24), (b) used Au/ZSM-5(DR-24) after 120 min reaction, (c) used Au/ZSM-5(DR-24) after 960 min reaction, (d) fresh Au/ZSM-5(DR-24-AHFS), (e) used Au/ZSM-5(DR-24-AHFS) after 120 min reaction, and (f) used Au/ZSM-5(DR-24-AHFS) after 960 min reaction. Reaction conditions: catalyst (0.1 g), CH_4 (20.7 bar), O_2 (3.5 bar), and H_2O (15 mL) at 240 °C.

24) catalyst, its reusability in methane oxidation was analyzed under optimized reaction conditions. Following the completion of the first reaction, the Au/ZSM-5(DR-24) catalyst was separated from the reaction mixture via centrifugation. Subsequently, it was washed with water and dried at 240 °C for 1.5 h before being reused in successive experiments. Remarkably, the catalyst demonstrates recyclability for five cycles while displaying only a marginal decline in methane oxidation performance (Figure 4d). This highlights the enhanced stability of the DR-treated catalyst compared to

https://doi.org/10.1021/acscatal.3c05030
ACS Catal. 2024, 14, 1797−1807

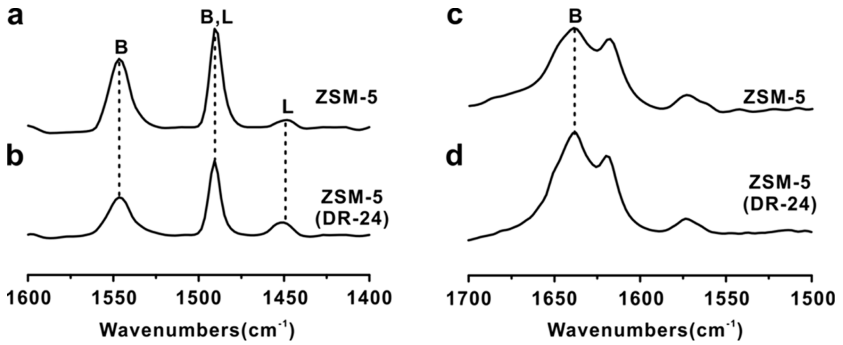

Figure 6. FTIR spectra of pyridine adsorbed on (a) ZSM-5 and (b) ZSM-5(DR-24), collidine adsorbed on (c) ZSM-5 and (d) ZSM-5(DR-24). The B and L peaks represent BASs and LASs, respectively.

Table 1. Acidity Property and Silicon and Aluminum Ratio of the Parent and DR-Treated ZSM-5 Zeolites[a]

entry	sample	Si/Al_{NMR}	acid concentration (μmol/g)				partially coordinated framework Al concentration (μmol/g)
			BAS			LAS	
			total	external	internal		
1	ZSM-5	25.7	431	67	364	32	15.4
2	ZSM-5(DR-24)	33.3	232	93	139	59	71.5
3	ZSM-5(DR-24-AHFS)	58.2	159	21	138	12	4.5

[a]Total BAS and LAS concentrations were obtained from the Py-IR experiments, the external BAS concentration was determined from the TMPy-IR experiments, and the internal BAS concentration was calculated by the subtraction of external BASs from the total BASs. The concentration of partially coordinated framework Al (PCFAL) was determined by multiplying the concentration of the total BASs by the proportion of PCFAL which was quantified by deconvolution of the 1D ^{27}Al MAS NMR spectra.

the previously studied Au/ZSM-5, which exhibited a consistent reduction in yield during recycled runs.[37] Taken together, these results suggest that the DR treatment applied to the ZSM-5 support enhances both the catalytic activity and the long-term stability of the catalyst during the reaction.

The fresh and used Au/ZSM-5(DR-24) catalyst was analyzed with HAADF-STEM to evaluate the effects of DR treatment on the supported Au species. As shown in Figure 5a–c, the Au nanoparticles retained an average size of approximately 10 nm following the reaction at 120 and 960 min. This indicates that there is little to no sintering of the Au particles during the reaction. In contrast, our previous work has shown the agglomeration of Au nanoparticles, during the methane oxidation reaction, when immobilized on an untreated ZSM-5 support (i.e., the Au/ZSM-5 catalyst), under identical reaction conditions.[37] The stability of Au nanoparticle in the case of the DR catalyst provides direct evidence explaining its enhanced resistance to deactivation through sintering over 2000 min of reaction time and multiple cycles. In metal-supported catalysts, a common occurrence is a decrease in catalyst activity as the supported metal particle size increases due to sintering. However, the DR formulation effectively bypasses this deactivation pathway by maintaining a high dispersion of catalytically active Au nanoparticles on the zeolite support.

Correlation of Catalyst Acidic Property to Methane Oxidation Reactivity. Based on previous work, the acidity of the zeolite support has been shown to significantly impact the activity of Au/ZSM-5 for methane oxidation.[37] Therefore, modification of the acidic properties of ZSM-5 through DR treatment may contribute to the improved catalytic performance of Au/ZSM-5. To test this, the acid sites of the parent ZSM-5 and ZSM-5(DR-24) samples were characterized using FT-IR spectroscopy with pyridine as a probe molecule (Figure 6). Pyridine is known to selectively interact with BASs and LASs, forming pyridinium ions or stable adsorbates, respectively. The IR spectra in Figure 6a,b reveal peaks characteristic of pyridine–BAS interactions at 1545 cm^{-1}, pyridine–LAS interactions at 1450 cm^{-1}, and a combined BAS/LAS signal at 1490 cm^{-1}. Quantitative analysis of the IR data, detailed in Table 1, shows that the DR treatment significantly decreases the BAS concentration from 431 to 232 μmol/g while increasing the LAS concentration from 32 to 59 μmol/g. Notably, despite having fewer BASs, the Au/ZSM-5(DR-24) catalyst exhibits superior methane oxidation activity compared to the untreated sample with higher BASs (Figures 3a and 4). This indicates that other acidity properties beyond simple BAS concentration, such as site location or Brønsted–Lewis character, also modulate the catalytic performance of Au/ZSM-5.

To gain insights into the spatial localization of acid sites, IR spectroscopy was also conducted using the bulky pyridine derivative 2,4,6-trimethylpyridine (TMPy), which is too large to penetrate the micropores of ZSM-5, enabling the measurement of acidity on the external surfaces of the zeolites.[42,43] The IR spectra of TMPy-exposed samples (Figure 6c,d) show a peak centered at 1639 cm^{-1} attributed to TMPy coordinated to the BAS on external surfaces. Quantitative analysis (Table 1) reveals the DR treatment increases the external BAS concentration from 67 to 93 μmol/g while decreasing the internal BAS concentration from 364 to 139 μmol/g. Such redistribution of BASs from internal to more accessible external positions resulting from DR likely contributes to the modified catalytic performance, given the improved access to acidic sites near Au particles and tunable metal–support interfacial interactions complex.

Given that the Al coordination state influences both zeolite acidity and Au anchoring capabilities, ^{27}Al MAS NMR was performed to probe the Al environments for both ZSM-5 supports (Figure S4). The parent ZSM-5 exhibits resonance

https://doi.org/10.1021/acscatal.3c05030
ACS Catal. 2024, 14, 1797–1807

primarily from tetrahedral framework aluminum (FAL) sites, along with minimal octahedral extra-framework aluminum (EFAL) signals. On the other hand, the ZSM-5 (DR-24) displays a decreased FAL component and emergence of pentahedral EFAL species. These ^{27}Al NMR observations corroborate the FT-IR acid site analysis, revealing dealumination and redistribution of Al species during DR treatment.

Since there is an increase of LAS due to EFAL species on ZSM-5(DR-24), we sought to probe the influence of EFAL on the catalyst activity. ZSM-5(DR-24) was treated with ammonium hexafluorosilicate (AHFS) to selectively extract EFAL,[44,45] yielding ZSM-5(DR-24-AHFS). FT-IR reveals significant decreases in LAS (from 59 to 12 μmol/g) and BAS (from 232 to 159 μmol/g) concentrations upon AHFS treatment (Table 1), with a greater impact on external (from 93 to 21 μmol/g) versus internal (from 139 to 138 μmol/g) BASs. Au/ZSM-5(DR-24-AHFS) catalyst was prepared with 0.5 wt % loading of Au and compared with Au-ZSM-5 and Au-ZSM-5(DR-24) for methane oxidation under the standard reaction conditions. As shown in Figure 7, the Au/ZSM-5(DR-24-AHFS) catalyst exhibits a lower methane oxidation activity than Au/ZSM-5 and Au/ZSM-5(DR-24) after both short-term (120 min) and long-term (960 min) reactions (Figure 7). This is expected, given that AHFS substantially reduced concentrations of both BASs and LASs. HAADF-STEM was used to analyze the Au nanoparticles on the fresh and spent Au/ZSM-5(DR-24-AHFS) catalyst. As shown in Figure 5d–f, the Au nanoparticles on Au/ZSM-5(DR-24-AHFS) increase in diameter following reactions at 120 and 960 min, in contrast no to little variation in particle size was observed for the Au/ZSM-5(DR-24) catalyst under identical conditions. The AHFS treatment thus renders Au nanoparticles on the modified ZSM-5 more susceptible to sintering during the methane oxidation reaction, likely reflecting weaker metal–support interactions and a loss of acid sites that could aid in nanoparticle stabilization against aggregation.

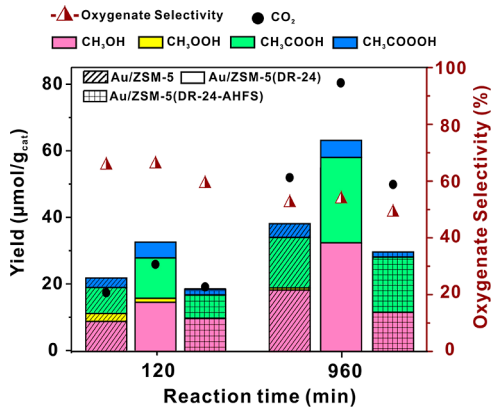

Figure 7. Methane oxidation activity of Au/ZSM-5, Au/ZSM-5(DR-24), and Au/ZSM-5(DR-24-AHFS). Reaction conditions: catalyst (0.1 g), CH_4 (20.7 bar), O_2 (3.5 bar), and H_2O (15 mL), 240 °C.

To discern the impact of specific acid site types, oxygenate yield after short- (120 min) and long-term (960 min) methane oxidation was plotted against the concentrations of total BASs and LASs (Figure 8) and external and internal BASs (Figure S5) for the three catalysts. No clear correlations are observed between oxygenate yield and concentration of these sites for either the initial or steady–state reaction (Figure 8a,d for total BASs; Figure 8b,e for LASs). This suggests the enhanced activity on DR-treated samples cannot be solely attributed to changes in the density or spatial distribution of traditionally characterized BASs or LASs.

The nature of the active site was further investigated by two-dimensional (2D) ^{27}Al multiple-quantum (MQ) MAS NMR spectroscopy. Figure 9 shows the 2D ^{27}Al MQ NMR spectra of ZSM-5, ZSM-5(DR-24) and ZSM-5(DR-24-AHFS). Three groups of tetrahedral FAl species are distinguished by their isotropic shifts of 53.1 ± 0.5 ppm (group 1), 55.4 ± 0.6 ppm (group 2), and 56.5 ± 1.0 ppm (group 3). The anisotropic slices along the F2 dimension reveal different quadrupolar product (PQ) parameters for each group, indicating different local environments of Al species. The PQ values for groups 1 and 2 are 2.1 MHz, while the PQ value for group 3 is 3.1 MHz. Groups 1 and 2 are assigned to BASs at different T-sites in the zeolite framework,[46] while group 3 can be attributed to partially coordinated framework Al (PCFAL) species,[47,48] which are considered to form as defects during the DR treatment. The proportion of PCFAL was estimated by deconvoluting the 1D ^{27}Al MAS NMR spectra using the isotropic chemical shifts and PQ parameters from the 2D MQ MAS NMR spectra (Figure 9 bottom and Table 1). The analysis was also performed on the spectra recorded at 500 MHz (Figure S6). It reveals that the ZSM-5(DR-24) sample contains the highest fraction of PCFAL at 30.8%. This was further confirmed by combining these NMR results with Py-IR, the concentration of PCFAL in the ZSM-5(DR-24) being determined to be 71.5 μmol/g (Table 1). In comparison, the unmodified parent ZSM-5 contains less PCFAL at 15.4 μmol/g. This type of Al site shows greater susceptibility to alteration by AHFS treatment, as evidenced by a significantly lower concentration of 4.5 μmol/g remained on the ZSM-5(DR-24-AHFS) sample. The PCFAL species may exhibit a more surface-oriented distribution on the zeolite, thereby experiencing greater modification upon exposure to the AHFS protocol, relative to Al sites residing deeper within the zeolitic framework. The elevated concentration of PCFAL species in ZSM-5(DR-24), relative to the parent ZSM-5 catalyst, likely contributed to its enhanced activity for methane oxidation.

To further explore the influence of PCFAL on catalytic performance, we analyzed the relationship between the oxygenate yield and PCFAL content for the three samples under examination (Figures 8c,f and S7). The strongest linear correlation was observed between oxygenate yield and PCFAL sites. This direct positive correlation provides strong evidence that partially bonded Al sites situated predominantly on the zeolite's external surface function to enhance methane oxidation. Previous studies have demonstrated that Al species exhibiting partial bonding within the zeolitic framework can enhance catalytic activity in catalytic processes such as benzene hydride transfer and *n*-hexane cracking.[31] As our previous density functional theory calculations for methane oxidation over Au/ZSM-5 illustrated, oxygen is preferentially adsorbed on Au nanoparticles to form active Au–O_2 complexes that facilitate methane activation.[37] The surface acidity arising from PCFAL could withdraw the electron density from the Au–O_2 complex, thereby lowering the transition state energy for the O–O bond scission and generating highly reactive oxygen species. Considering the aforementioned TEM analysis indicating stabilization of Au nanoparticle size on DR-treated zeolite, the surface location of PCFAL appears to also hinder

https://doi.org/10.1021/acscatal.3c05030
ACS Catal. 2024, 14, 1797–1807

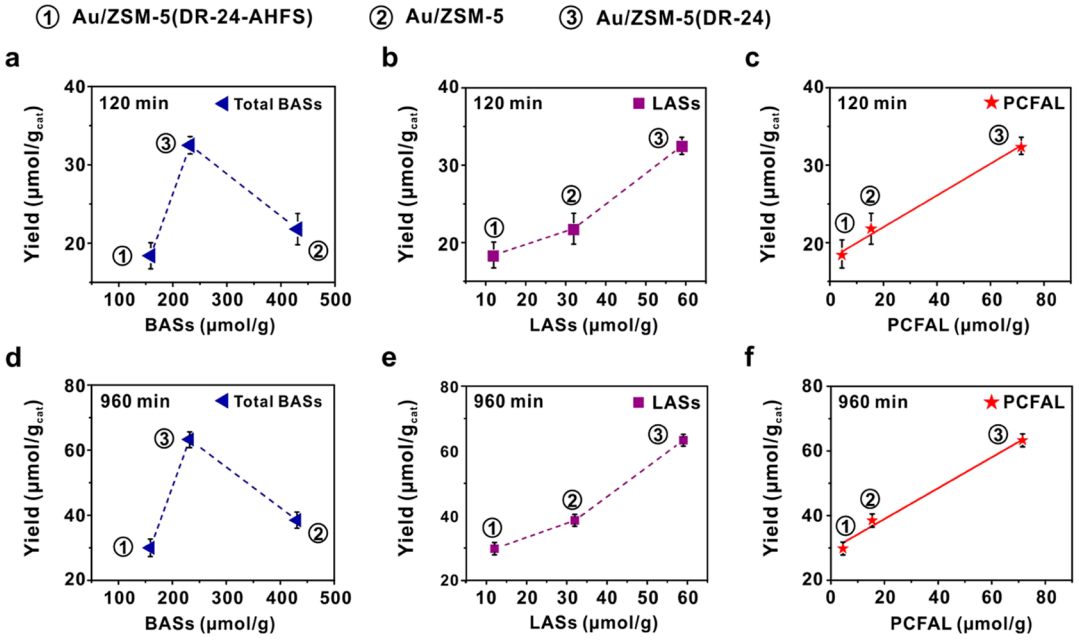

Figure 8. Oxygenate yield of methane oxidation against the concentration of total BASs, LASs, and PCFAL on three catalysts at different reaction times of (a−c) 120 and (d−f) 960 min. Error bars were obtained from triplicate measurements. Reaction conditions: catalyst (0.1 g), CH_4 (20.7 bar), O_2 (3.5 bar), and H_2O (15 mL), 240 °C.

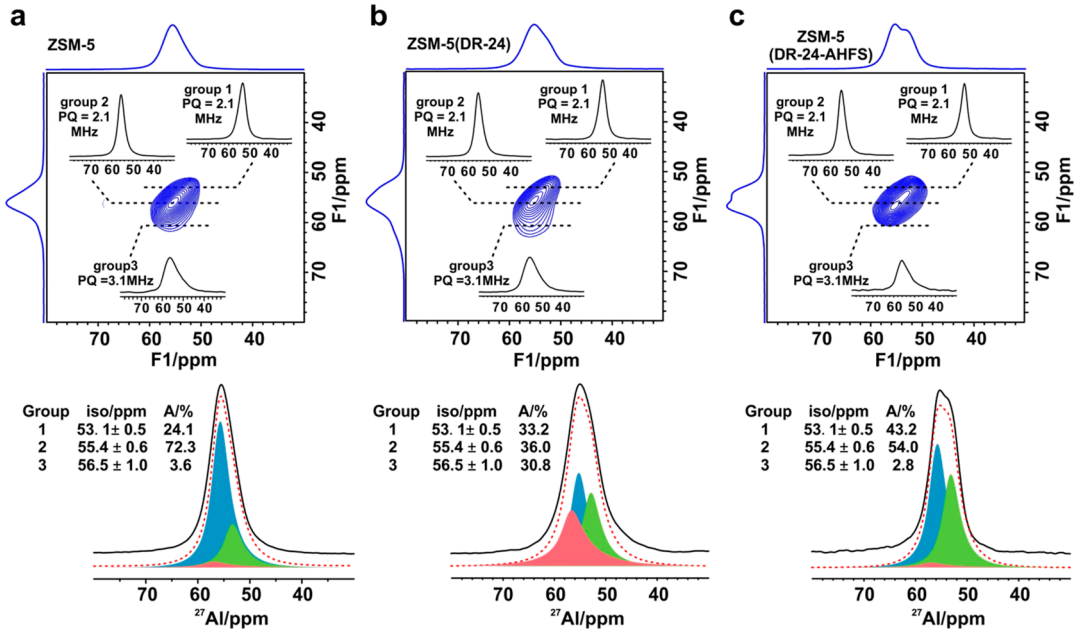

Figure 9. ^{27}Al 3QMAS NMR spectra of (a) ZSM-5, (b) ZSM-5(DR-24), and (c) ZSM-5(DR-24-AHFS) at 800 MHz with summed projections in both dimensions and the extracted 1D slices along the direction parallel to the F2 dimension in insets. Experimental and simulated ^{27}Al MAS NMR spectra at the bottom show the proportion of Al sites in different groups.

Au agglomeration by strengthening metal−support interactions between Au nanoparticles and the zeolite surface. This enhanced interfacial contact contributes to improved catalytic stability through resistance against sintering of the supported Au species, conferring benefits for methane oxidation performance over extended reaction times.

CONCLUSIONS

This work investigated the effects of a DR treatment on the activity and stability of Au/ZSM-5 catalysts for the direct oxidation of methane to oxygenates. The modified zeolite support offers up to 50% higher liquid oxygenate yield (mainly methanol and acetic acid) compared to the unmodified catalyst, with a maintained yield and stability over time. We demonstrate how acid site speciation and distribution changed with DR treatment. FTIR and ^{27}Al NMR show the total BASs decrease due to a reduction inside zeolite channels, while the BASs become enriched on the external surface. 2D ^{27}Al MQMAS NMR further identifies more partially coordinated framework aluminum sites on the DR sample, correlating to both higher oxygenate yield and promoted catalyst lifetime due to stabilization of supported Au nanoparticles. The results

https://doi.org/10.1021/acscatal.3c05030
ACS Catal. 2024, 14, 1797−1807

provide insight into modifying zeolite supports to enhance the methane conversion performance and stability through the redistribution and coordination of acid sites. The findings offer a viable strategy for an efficient catalyst design in this reaction.

■ ASSOCIATED CONTENT

Supporting Information

The Supporting Information is available free of charge at https://pubs.acs.org/doi/10.1021/acscatal.3c05030.

Data relating to catalytic activity toward the selective oxidation of methane, with accompanying characterization of catalysts via BET, TEM, and ^{27}Al solid-state NMR (PDF)

■ AUTHOR INFORMATION

Corresponding Authors

Graham J. Hutchings − *Max Planck−Cardiff Centre on the Fundamentals of Heterogeneous Catalysis FUNCAT, Cardiff Catalysis Institute, School of Chemistry, Cardiff University Translational Research Hub, Cardiff CF24 4HQ, U.K.;* orcid.org/0000-0001-8885-1560; Email: Hutch@cardiff.ac.uk

Jun Xu − *National Centre for Magnetic Resonance in Wuhan, State Key Laboratory of Magnetic Resonance and Atomic and Molecular Physics, Innovation Academy for Precision Measurement Science and Technology, Chinese Academy of Sciences, Wuhan 430071, China; University of Chinese Academy of Sciences, Beijing 100049, China;* orcid.org/0000-0003-2741-381X; Email: xujun@wipm.ac.cn

Authors

Jingxian Cao − *National Centre for Magnetic Resonance in Wuhan, State Key Laboratory of Magnetic Resonance and Atomic and Molecular Physics, Innovation Academy for Precision Measurement Science and Technology, Chinese Academy of Sciences, Wuhan 430071, China; University of Chinese Academy of Sciences, Beijing 100049, China*

Guodong Qi − *National Centre for Magnetic Resonance in Wuhan, State Key Laboratory of Magnetic Resonance and Atomic and Molecular Physics, Innovation Academy for Precision Measurement Science and Technology, Chinese Academy of Sciences, Wuhan 430071, China; University of Chinese Academy of Sciences, Beijing 100049, China*

Bingqing Yao − *National University of Singapore, Singapore 117575, Singapore*

Qian He − *National University of Singapore, Singapore 117575, Singapore;* orcid.org/0000-0003-4891-3581

Richard J. Lewis − *Max Planck−Cardiff Centre on the Fundamentals of Heterogeneous Catalysis FUNCAT, Cardiff Catalysis Institute, School of Chemistry, Cardiff University Translational Research Hub, Cardiff CF24 4HQ, U.K.;* orcid.org/0000-0001-9990-7064

Xu Li − *National Centre for Magnetic Resonance in Wuhan, State Key Laboratory of Magnetic Resonance and Atomic and Molecular Physics, Innovation Academy for Precision Measurement Science and Technology, Chinese Academy of Sciences, Wuhan 430071, China; University of Chinese Academy of Sciences, Beijing 100049, China*

Feng Deng − *National Centre for Magnetic Resonance in Wuhan, State Key Laboratory of Magnetic Resonance and Atomic and Molecular Physics, Innovation Academy for Precision Measurement Science and Technology, Chinese Academy of Sciences, Wuhan 430071, China; University of Chinese Academy of Sciences, Beijing 100049, China;* orcid.org/0000-0002-6461-7152

Complete contact information is available at: https://pubs.acs.org/10.1021/acscatal.3c05030

Author Contributions

The manuscript was written through contributions of all authors. All authors have given approval to the final version of the manuscript.

Notes

The authors declare no competing financial interest.

■ ACKNOWLEDGMENTS

This work was financially supported by the National Key R&D Program of China (2022YFA1504500), the National Natural Science Foundation of China (22272185, 22320102002, 22225205, 22127801 and U1932218), and the Natural Science Foundation of Hubei Province (S22H120101). J.X. thanks the Royal Society and the Newton Fund for the Royal Society-Newton Advanced Fellowship (NAF\R1\201066). G.J.H. acknowledges the support from the Chinese Academy of Sciences (CAS) President's International Fellowship Initiative (PIFI) (grant no. 2019DM0015). Q.H. thanks the support from the National Research Foundation (NRF) Singapore, under its NRF Fellowship (NRF-NRFF11-2019-0002). R.J.L. and G.J.H. thank Cardiff University and the Max Planck Centre for Fundamental Heterogeneous Catalysis (FUNCAT) for financial support.

■ REFERENCES

(1) Wang, V. C. C.; Maji, S.; Chen, P. P. Y.; Lee, H. K.; Yu, S. S. F.; Chan, S. I. Alkane oxidation: methane monooxygenases, related enzymes, and their biomimetics. *Chem. Rev.* **2017**, *117*, 8574−8621.

(2) Latimer, A. A.; Kakekhani, A.; Kulkarni, A. R.; Norskov, J. K. Direct methane to methanol: the selectivity-conversion limit and design strategies. *ACS Catal.* **2018**, *8*, 6894−6907.

(3) Li, S.; Ahmed, R.; Yi, Y.; Bogaerts, A. Methane to methanol through heterogeneous catalysis and plasma catalysis. *Catalysts* **2021**, *11*, 590.

(4) Meng, X.; Cui, X.; Rajan, N. P.; Yu, L.; Deng, D.; Bao, X. Direct methane conversion under mild condition by thermo-electro-or photocatalysis. *Chem* **2019**, *5*, 2296−2325.

(5) Periana, R. A.; Taube, D. J.; Gamble, S.; Taube, H.; Satoh, T.; Fujii, H. Platinum catalysts for the high-yield oxidation of methane to a methanol derivative. *Science* **1998**, *280*, 560−564.

(6) Tomkins, P.; Ranocchiari, M.; Van Bokhoven, J. A. Direct conversion of methane to methanol under mild conditions over Cu-zeolites and beyond. *Acc. Chem. Res.* **2017**, *50*, 418−425.

(7) Latimer, A. A.; Kulkarni, A. R.; Aljama, H.; Montoya, J. H.; Yoo, J. S.; Tsai, C.; Abild-Pedersen, F.; Studt, F.; Nørskov, J. K. Understanding trends in C-H bond activation in heterogeneous catalysis. *Nat. Mater.* **2017**, *16*, 225−229.

(8) Hickman, D. A.; Schmidt, L. D. Production of syngas by direct catalytic-oxidation of methane. *Science* **1993**, *259*, 343−346.

(9) Conley, B. L.; Tenn, W. J., III; Young, K. J. H.; Ganesh, S. K.; Meier, S. K.; Ziatdinov, V. R.; Mironov, O.; Oxgaard, J.; Gonzales, J.; Goddard, W. A., III; Periana, R. A. Design and study of homogeneous catalysts for the selective, low temperature oxidation of hydrocarbons. *J. Mol. Catal. A: Chem.* **2006**, *251*, 8−23.

(10) Kwon, Y.; Kim, T. Y.; Kwon, G.; Yi, J.; Lee, H. Selective activation of methane on single-atom catalyst of Rhodium dispersed on Zirconia for direct conversion. *J. Am. Chem. Soc.* **2017**, *139*, 17694−17699.

(11) Huang, W.; Zhang, S.; Tang, Y.; Li, Y.; Nguyen, L.; Li, Y.; Shan, J.; Xiao, D.; Gagne, R.; Frenkel, A. I.; Tao, F. Low-temperature transformation of methane to methanol on Pd_1O_4 single sites anchored on the internal surface of microporous silicate. *Angew. Chem., Int. Ed.* **2016**, *55*, 13441−13445.
(12) Dummer, N. F.; Willock, D. J.; He, Q.; Howard, M. J.; Lewis, R. J.; Qi, G.; Taylor, S. H.; Xu, J.; Bethell, D.; Kiely, C. J.; Hutchings, G. J. Methane oxidation to methanol. *Chem. Rev.* **2023**, *123*, 6359−6411.
(13) Wang, S.; Fung, V.; Hülsey, M. J.; Liang, X.; Yu, Z.; Chang, J.; Folli, A.; Lewis, R. J.; Hutchings, G. J.; He, Q.; Yan, N. H_2-reduced phosphomolybdate promotes room-temperature aerobic oxidation of methane to methanol. *Nat. Catal.* **2023**, *6*, 895−905.
(14) Mao, J.; Liu, H.; Cui, X.; Zhang, Y.; Meng, X.; Zheng, Y.; Chen, M.; Pan, Y.; Zhao, Z.; Hou, G.; Hu, J.; Li, Y.; Xu, G.; Huang, R.; Yu, L.; Deng, D. Direct conversion of methane with O_2 at room temperature over edge-rich MoS_2. *Nat. Catal.* **2023**, *6*, 1052−1061.
(15) Periana, R. A.; Taube, D. J.; Evitt, E. R.; Loffler, D. G.; Wentrcek, P. R.; Voss, G.; Masuda, T. A mercury-catalyzed, high-yield system for the oxidation of methane to methanol. *Science* **1993**, *259*, 340−343.
(16) Ab Rahim, M. H.; Forde, M. M.; Jenkins, R. L.; Hammond, C.; He, Q.; Dimitratos, N.; Lopez-Sanchez, J. A.; Carley, A. F.; Taylor, S. H.; Willock, D. J.; Murphy, D. M.; Kiely, C. J.; Hutchings, G. J. Oxidation of methane to methanol with hydrogen peroxide using supported gold-palladium alloy nanoparticles. *Angew. Chem., Int. Ed.* **2013**, *52*, 1280−1284.
(17) Williams, C.; Carter, J. H.; Dummer, N. F.; Chow, Y. K.; Morgan, D. J.; Yacob, S.; Serna, P.; Willock, D. J.; Meyer, R. J.; Taylor, S. H.; Hutchings, G. J. Selective oxidation of methane to methanol using supported AuPd catalysts prepared by stabilizer-free sol-immobilization. *ACS Catal.* **2018**, *8*, 2567−2576.
(18) Shan, J.; Li, M.; Allard, L. F.; Lee, S.; Flytzani-Stephanopoulos, M. Mild oxidation of methane to methanol or acetic acid on supported isolated rhodium catalysts. *Nature* **2017**, *551*, 605−608.
(19) Hammond, C.; Forde, M. M.; Ab Rahim, M. H.; Thetford, A.; He, Q.; Jenkins, R. L.; Dimitratos, N.; Lopez-Sanchez, J. A.; Dummer, N. F.; Murphy, D. M.; Carley, A. F.; Taylor, S. H.; Willock, D. J.; Stangland, E. E.; Kang, J.; Hagen, H.; Kiely, C. J.; Hutchings, G. J. Direct Catalytic Conversion of Methane to Methanol in an Aqueous Medium by using Copper-Promoted Fe-ZSM-5. *Angew. Chem., Int. Ed.* **2012**, *51*, 5129−5133.
(20) Yu, T.; Li, Z.; Lin, L.; Chu, S.; Su, Y.; Song, W.; Wang, A.; Weckhuysen, B. M.; Luo, W. Highly Selective Oxidation of Methane into Methanol over Cu-Promoted Monomeric Fe/ZSM-5. *ACS Catal.* **2021**, *11*, 6684−6691.
(21) Agarwal, N.; Freakley, S. J.; McVicker, R. U.; Althahban, S. M.; Dimitratos, N.; He, Q.; Morgan, D. J.; Jenkins, R. L.; Willock, D. J.; Taylor, S. H.; Kiely, C. J.; Hutchings, G. J. Aqueous Au-Pd colloids catalyze selective CH_4 oxidation to CH_3OH with O_2 under mild conditions. *Science* **2017**, *358*, 223−227.
(22) Wu, B.; Lin, T.; Lu, Z.; Yu, X.; Huang, M.; Yang, R.; Wang, C.; Tian, C.; Li, J.; Sun, Y.; Zhong, L. Fe binuclear sites convert methane to acetic acid with ultrahigh selectivity. *Chem* **2022**, *8*, 1658−1672.
(23) Cui, X.; Li, H.; Wang, Y.; Hu, Y.; Hua, L.; Li, H.; Han, X.; Liu, Q.; Yang, F.; He, L.; Chen, X.; Li, Q.; Xiao, J.; Deng, D.; Bao, X. Room-temperature methane conversion by graphene-confined single Iron atoms. *Chem* **2018**, *4*, 1902−1910.
(24) Zhu, K.; Liang, S.; Cui, X.; Huang, R.; Wan, N.; Hua, L.; Li, H.; Chen, H.; Zhao, Z.; Hou, G.; Li, M.; Jiang, Q.; Yu, L.; Deng, D. Highly efficient conversion of methane to formic acid under mild conditions at ZSM-5-confined Fe-sites. *Nano Energy* **2021**, *82*, 105718.
(25) Jin, Z.; Wang, L.; Zuidema, E.; Mondal, K.; Zhang, M.; Zhang, J.; Wang, C.; Meng, X.; Yang, H.; Mesters, C.; Xiao, F. Hydrophobic zeolite modification for in situ peroxide formation in methane oxidation to methanol. *Science* **2020**, *367*, 193−197.
(26) Wu, B.; Lin, T.; Huang, M.; Li, S.; Li, J.; Yu, X.; Yang, R.; Sun, F.; Jiang, Z.; Sun, Y.; Zhong, L. Tandem catalysis for selective oxidation of methane to oxygenates using oxygen over PdCu/zeolite. *Angew. Chem., Int. Ed.* **2022**, *61*, No. e202204116.
(27) Tang, Y.; Li, Y.; Fung, V.; Jiang, D. E.; Huang, W.; Zhang, S.; Iwasawa, Y.; Sakata, T.; Nguyen, L.; Zhang, X.; Frenkel, A. I.; Tao, F. Single rhodium atoms anchored in micropores for efficient transformation of methane under mild conditions. *Nat. Commun.* **2018**, *9*, 1231.
(28) Narsimhan, K.; Iyoki, K.; Dinh, K.; Roman-Leshkov, Y. Catalytic oxidation of methane into methanol over copper-exchanged zeolites with oxygen at low temperature. *ACS Cent. Sci.* **2016**, *2*, 424−429.
(29) Dinh, K. T.; Sullivan, M. M.; Narsimhan, K.; Serna, P.; Meyer, R. J.; Dincă, M.; Roman-Leshkov, Y. Continuous partial oxidation of methane to methanol catalyzed by diffusion-paired copper dimers in copper-exchanged zeolites. *J. Am. Chem. Soc.* **2019**, *141*, 11641−11650.
(30) Koishybay, A.; Shantz, D. F. Water is the oxygen source for methanol produced in partial oxidation of methane in a flow reactor over Cu-SSZ-13. *J. Am. Chem. Soc.* **2020**, *142*, 11962−11966.
(31) Sun, L.; Wang, Y.; Wang, C.; Xie, Z.; Guan, N.; Li, L. Water-involved methane-selective catalytic oxidation by dioxygen over copper zeolites. *Chem* **2021**, *7*, 1557−1568.
(32) Groothaert, M. H.; Smeets, P. J.; Sels, B. F.; Jacobs, P. A.; Schoonheydt, R. A. Selective Oxidation of Methane by the Bis(μ-oxo)dicopper Core Stabilized on ZSM-5 and Mordenite Zeolites. *J. Am. Chem. Soc.* **2005**, *127*, 1394−1395.
(33) Narsimhan, K.; Michaelis, V. K.; Mathies, G.; Gunther, W. R.; Griffin, R. G.; Román-Leshkov, Y. Methane to acetic acid over Cu-exchanged zeolites: mechanistic insights from a site-specific carbonylation reaction. *J. Am. Chem. Soc.* **2015**, *137*, 1825−1832.
(34) Tomkins, P.; Mansouri, A.; Bozbag, S. E.; Krumeich, F.; Park, M. B.; Alayon, E. M. C.; Ranocchiari, M.; van Bokhoven, J. A. Isothermal cyclic conversion of methane into methanol over copper-exchanged zeolite at low temperature. *Angew. Chem., Int. Ed.* **2016**, *55*, 5467−5471.
(35) Grundner, S.; Markovits, M. A. C.; Li, G.; Tromp, M.; Pidko, E. A.; Hensen, E. J. M.; Jentys, A.; Sanchez-Sanchez, M.; Lercher, J. A. Single-site trinuclear copper oxygen clusters in mordenite for selective conversion of methane to methanol. *Nat. Commun.* **2015**, *6*, 7546.
(36) Smeets, P. J.; Groothaert, M. H.; Schoonheydt, R. A. Cu based zeolites: a UV-vis study of the active site in the selective methane oxidation at low temperatures. *Catal. Today* **2005**, *110*, 303−309.
(37) Qi, G.; Davies, T. E.; Nasrallah, A.; Sainna, M. A.; Howe, A. G. R.; Lewis, R. J.; Quesne, M.; Catlow, C. R. A.; Willock, D. J.; He, Q.; Bethell, D.; Howard, M. J.; Murrer, B. A.; Harrison, B.; Kiely, C. J.; Zhao, X.; Deng, F.; Xu, J.; Hutchings, G. J. Au-ZSM-5 catalyses the selective oxidation of CH_4 to CH_3OH and CH_3COOH using O_2. *Nat. Catal.* **2022**, *5*, 45−54.
(38) Steinhauser, G.; Evers, J.; Jakob, S.; Klapotke, T. M.; Oehlinger, G. A review on fulminating gold (Knallgold). *Gold Bull.* **2008**, *41*, 305−317.
(39) Cooper, C. M.; Wiezevich, P. J. Effects of temperature and pressure on the upper explosive limit of methane-oxygen mixtures. *Ind. Eng. Chem.* **1929**, *21*, 1210−1214.
(40) Massiot, D.; Fayon, F.; Capron, M.; King, I.; Le Calvé, S.; Alonso, B.; Durand, J. O.; Bujoli, B.; Gan, Z. H.; Hoatson, G. Modelling one- and two-dimensional solid-state NMR spectra. *Magn. Reson. Chem.* **2002**, *40*, 70−76.
(41) Cao, J.; Lewis, R. J.; Qi, G.; Bethell, D.; Howard, M. J.; Harrison, B.; Yao, B.; He, Q.; Morgan, D. J.; Ni, F. L.; Sharma, P.; Kiely, C. J.; Li, X.; Deng, F.; Xu, J.; Hutchings, G. J. Methane conversion to methanol using Au/ZSM-5 is promoted by carbon. *ACS Catal.* **2023**, *13*, 7199−7209.
(42) Holm, M. S.; Svelle, S.; Joensen, F.; Beato, P.; Christensen, C. H.; Bordiga, S.; Bjorgen, M. Assessing the acid properties of desilicated ZSM-5 by FTIR using CO and 2,4,6-trimethylpyridine (collidine) as molecular probes. *Appl. Catal., A* **2009**, *356*, 23−30.
(43) Thibault-Starzyk, F.; Stan, I.; Abello, S.; Bonilla, A.; Thomas, K.; Fernandez, C.; Gilson, J. P.; Perez-Ramirez, J. Quantification of

https://doi.org/10.1021/acscatal.3c05030
ACS Catal. 2024, 14, 1797−1807

enhanced acid site accessibility in hierarchical zeolites - the accessibility index. *J. Catal.* **2009**, *264*, 11−14.
(44) Hu, M.; Wang, C.; Chu, Y.; Wang, Q.; Li, S.; Xu, J.; Deng, F. Unravelling the reactivity of framework Lewis acid sites towards methanol activation on H-ZSM-5 zeolite with solid-state NMR spectroscopy. *Angew. Chem., Int. Ed.* **2022**, *61*, No. e202207400.
(45) Maijanen, A.; Derouane, E. G.; Nagy, J. B. FT-IR and solid-state NMR investigation of surface hydroxyl-groups on dealuminated ZSM-5. *Appl. Surf. Sci.* **1994**, *75*, 204−212.
(46) Holzinger, J.; Beato, P.; Lundegaard, L. F.; Skibsted, J. Distribution of aluminum over the tetrahedral sites in ZSM-5 zeolites and their evolution after steam treatment. *J. Phys. Chem. C* **2018**, *122*, 15595−15613.
(47) Chen, K.; Horstmeier, S.; Nguyen, V. T.; Wang, B.; Crossley, S. P.; Pham, T.; Gan, Z.; Hung, I.; White, J. L. Structure and Catalytic Characterization of a Second Framework Al(IV) Site in Zeolite Catalysts Revealed by NMR at 35.2 T. *J. Am. Chem. Soc.* **2020**, *142*, 7514−7523.
(48) Chen, K.; Gan, Z.; Horstmeier, S.; White, J. L. Distribution of Aluminum Species in Zeolite Catalysts: ^{27}Al NMR of Framework, Partially-Coordinated Framework, and Non-Framework Moieties. *J. Am. Chem. Soc.* **2021**, *143*, 6669−6680.

https://doi.org/10.1021/acscatal.3c05030
ACS Catal. 2024, 14, 1797−1807